Geotechnical and Geophysical Site Characterization – Huang & Mayne (eds)
© 2008 Taylor & Francis Group, London, ISBN 978-0-415-46936-4

Seismic cross-hole tomography in modeling ISC'2 experimental site

J.M. Carvalho & A. Viana da Fonseca
Universidade do Porto – Faculdade de Engenharia, Porto, Portugal

F. Almeida
Universidade de Aveiro – Departamento de Geociências, Campus de Santiago, Aveiro, Portugal

ABSTRACT: The extensive in-situ investigation and characterization of ISC'2 experimental site, located on the campus of the Faculty of Engineering of the University of Porto (FEUP), comprised a geological reconnaissance of the area as well as the application of several geophysical and geotechnical surface and borehole methods, namely seismic P- and S-wave seismic refraction, conventional and tomographic cross-hole, high resolution SH-wave shallow reflection, geoelectrical resistivity imaging, penetration tests and pressure-dilatometer tests. In parallel, a laboratory testing program was carried out on undisturbed samples, including triaxial tests with bender elements and resonant column tests. Broadly, the site is geologically formed by an upper layer of soil with varying thickness, overlaying rather weathered granite (saprolite) contacting an older gneissic migmatite having dominant sub-vertical foliation, with the piezometric water level at a depth about 10 m during the surveying period. Direct and indirect results from some of the referred geophysical surveys, namely those obtained from seismic refraction and reflection, conventional cross-hole, down-hole, geoelectrical imaging and ground penetrating radar, as well as from the geotechnical in-situ and laboratory tests, have been previously presented, compared and discussed. Following a brief summary of some relevant contextualizing issues, the present report presents and discusses results obtained from the conducted seismic cross-hole tomography survey as well as their integration in the previously obtained tentative ISC'2 experimental soil profile interpretation model.

1 INTRODUCTION

1.1 *Outline*

The geological reconnaissance of ISC'2 experimental site, the application of numerous geophysical and geotechnical surface and borehole methods as well as the laboratory tests carried on, yielded a significant database for subsequent treatment and interpretation.

Different objectives were then fixed, namely: assessment of the adequacy for the site characterization of single methods/tests; assessment of the consistency among results from different methods/tests; correlations/regression models between results of single methods/tests; data integration from different methods/tests aiming at obtaining a consistent and reliable geological/geotechnical interpretation model.

Several results have been previously reported and discussed (Viana da Fonseca et al., 2006). However, data acquired for subsequent seismic cross-hole (CH) velocity inversion had not yet been processed. In addition, complementary data treatment approaches may help to enlighten previously obtained results, leading to a better understanding of their subjacent fundaments. In the present paper the focus will be made in these two referred perspectives: integration of additional data in the previously deduced S-wave models and the use of additional data treatment procedures in both previously and presently treated conventional and tomographic CH data.

1.2 *Geology*

In Porto area where the site is located, fresh outcroppings of basement rocks are rare, being the site geologically formed by upper soil layers of varying thickness, overlaying a more or less weathered granite contacting an older gneissic migmatite, with dominant sub-vertical foliation.

Generically, the basement lithologies – granite and metamorphic rocks including high grade schist, gneiss and migmatite – are strongly deformed and metamorphosed.

The thickness of these residual saprolitic horizons can vary from few meters to more than 20 m, often combining a strong "random" component of spatial variability/heterogeneity, with a frequently observed "deterministic" trend through depth, namely regarding their hydraulic and mechanical properties.

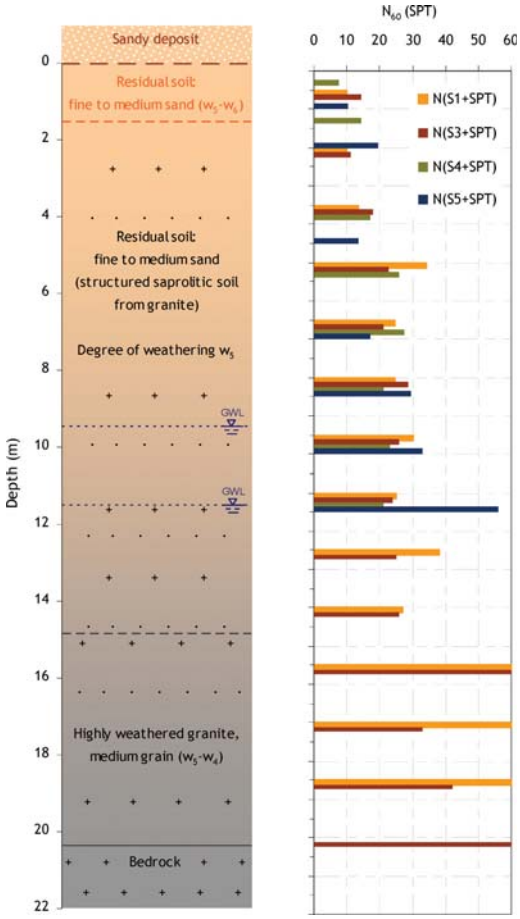

Figure 1. Schematic geological profile and N_{SPT} values from boreholes S1, S3, S4 and S5 (Viana da Fonseca et al., 2006).

Laboratory tests on locally collected undisturbed samples have classified the soil as clayey silty sand. The following average values for the strength parameters were derived: friction angle $\phi' = 45.8°$ and cohesion $c' = 4.5$ KPa (Viana da Fonseca et al., 2006).

Figure 1 shows a schematic site geological profile and N_{60} SPT values from nearby boreholes S1, S3, S4 and S5.

2 SEISMIC CROSS-HOLE

2.1 *Conventional cross-hole*

Three PVC cased boreholes, S1, S2 and S3 (Fig. 2), were used for a S- and P-wave CH survey.

Field equipment comprised a Soil Dynamics mechanical bidirectional vertical borehole hammer with a central frequency of 400 Hz and a Geo-Stuff

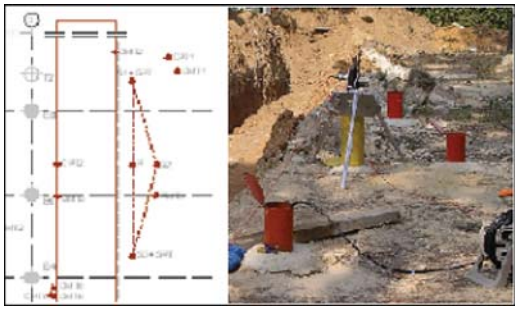

Figure 2. S1, S2 and S3 boreholes location at FEUP experimental site.

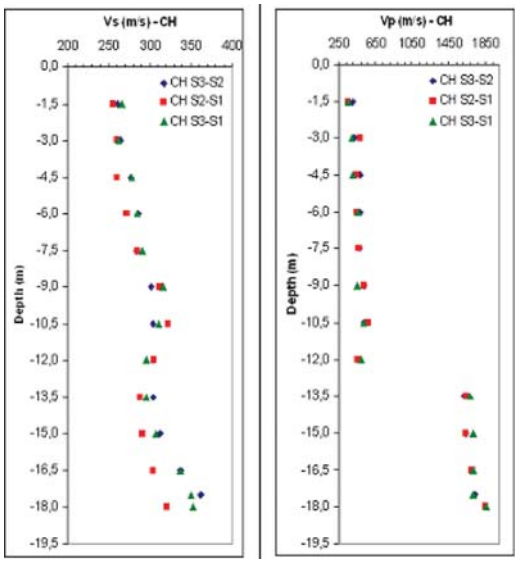

Figure 3. CH V_S and V_P profiles, in sections S1-S2, S2-S3 and S1-S3.

BHG-3 14 Hz triaxial geophone system, coupled to a Geometrics Smartseis 12 channel seismograph.

Figure 3 presents V_S and V_P profiles obtained in the referred three sections.

Acquisition was carried out between boreholes S1-S2, S2-S3 and S1-S3, defining three sections, respectively, 4.25 m, 4.35 and 8.4 m wide, going to a maximum depth of 18 m.

Generically all three sections have a very similar velocity profile pattern, being each one very much representative of the others, although quite distinctive between V_S and V_P: V_S profile trend corresponds to an average gradual increase of velocity with depth, varying from minimum values about 260 m/s to maximum values about 360 m/s. V_P profile has a clear discontinuity between 12 m (about 500 m/s) and 13,5 m (about 1600 m/s) depths, presumably due to the transition

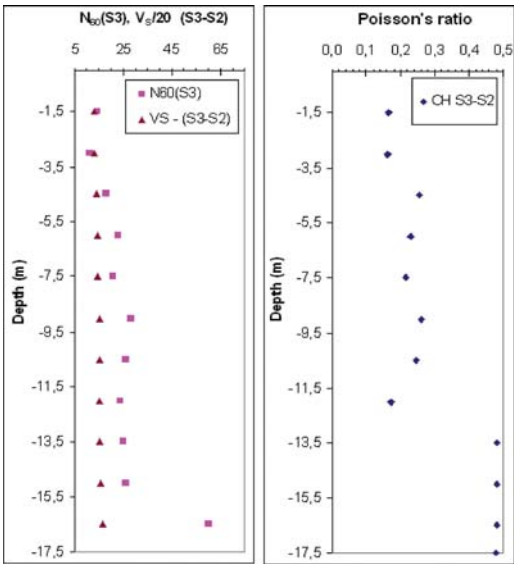

Figure 4. Left: profiles of scaled (divided by 20) SPT N_{60} values from borehole S3 and V_S from section S3-S2; Right: section S3-S2 Poisson ratio profile.

between partial to full soil saturation, (Berge, P. & Bonner, B., 2002).

In the left part of Figure 4, N_{60} SPT values from borehole S3 are compared with scaled (divided by 20) V_S values from section S3-S2, showing a very similar variability in depth.

Dynamic Poisson ratio (ν) was estimated from V_P and V_S values. In the right part of Figure 4, ν values from section S3-S2 are plotted, varying around an average value of 0.25 above 13,5 m and being quite constant below that level with values close to 0.5 which is also a sign of full saturation.

The calculated G_0 values vary, fairly smoothly, between 120 MPa to about 255 MPa.

Initial results obtained with CH data collected in section S3-S2, having in mind the subsequent tomographic processing and interpretation, will be next presented and discussed.

2.2 *Tomographic cross-hole*

Data acquisition in section S3-S2 was carried out over a depth interval from 1.5 m to 17.5 m with a vertical spacing of 1.5 m except the deeper one of 1 m, due to the borehole base. The energy was generated with a borehole hammer designed to generate mainly S-waves vertically polarized propagating horizontally, S_{HV}, especially adequate to S-wave conventional CH.

Acquisition for subsequent velocity inversion implies a significant change in conditions whose repercussions in the recorded seismograms should be taken into consideration and well understood for an accurate data treatment and interpretation. Several different seismic events may occur, namely wave conversions, reflections, refractions, scattering and tube waves, (Wang Y, & Rao, Y., 2006).

Aiming at reducing the inherent ambiguity, data processing of CH section S3-S2 went through the following steps:

- Picking of direct S-waves first arrivals in each individual conventional CH trace;
- Direct import of data to Sandmeier software Reflex;
- Sorting: data separation by shot and component (radial, R, transversal, T, vertical, V);
- Edition of the geometry: for each created shot-gather, record sequencing according to respective depth;
- Filtering: three different sets were considered – no-filtering; high bandpath filtering 150–500 Hz (HPB) and low bandpath filtering 5–150 Hz (LPB);
- Time/distance, T-X, graphs display: with and without trace normalization;
- Print screen crop of T-X graph windows to Excel environment;
- Modeling of seismic events: for the different interpreted main seismic events observed in each shot-gather, correspondent first arrivals fitting by hyperbolae representing theoretical models arrival times;
- Picking of first arrivals in each individual trace.

Figure 5 shows the receiver-gather of the 12 vertical component non filtered traces for shot-point at depth 13,5 m.

The fitted hyperbolic models are related to the following theoretical seismic events: P- and S-wave direct, respectively tPD and tSd, and reflected first arrivals at the soil/air interface, tSs, and soil/bedrock interface, tSb, assumed to be located at 18,5 m depth. The referred events interpreted as reflections, are much more clear in processed records, namely in those shown in Figures 8 and 10. The hyperbolic models simulating the reflected mentioned events are globally better fitted with average V_S and V_P values, rather than with conventional CH data, since they are not constant within the section.

The upper P-wave hyperbolic model uses $V_P =$ 1620 m/s obtained for this depth, fitting the high frequency first arrivals event, which is very clear in the picture right upper corner. These events, although containing above 750 Hz high frequency amplitudes, in the geophone spurious frequency range, are interpreted as being mostly related to coherent P-wave energy effects.

The normalized spectrogram of Figure 6 graphically shows the time varying frequency content of the transversal component of the CH trace corresponding to depth 13,5 m where the conventional CH first

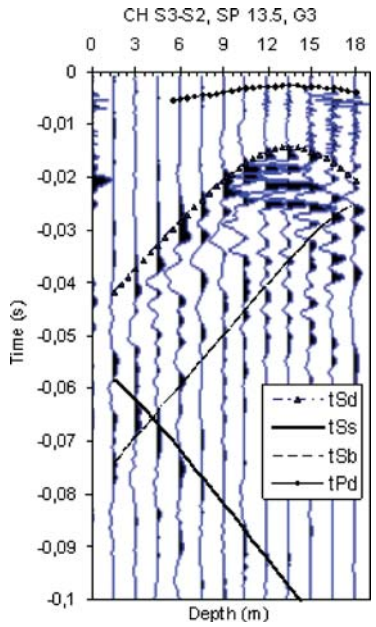

Figure 5. Shot-point 13,5 m vertical component receiver-gather (normalized non filtered traces) overlaid by model hyperbolae.

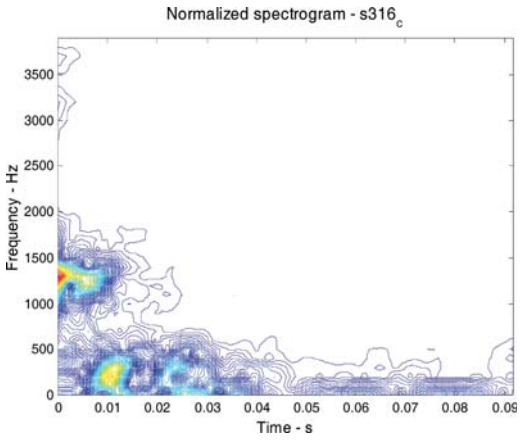

Figure 6. Spectrogram of the transversal component of the CH 13,5 m depth trace.

clearly detected water related P-wave velocities. It is possible to identify clearly a high frequency range (1000–1500 Hz) for the early event arrival, which is not present in the spectrogram of the vertical component (Figure 7).

These events appear to be the most reliable sign of soil full saturation, appearing in the traces below depth 13,5 m. Looking at the CH V_S profile (Fig. 3) depth

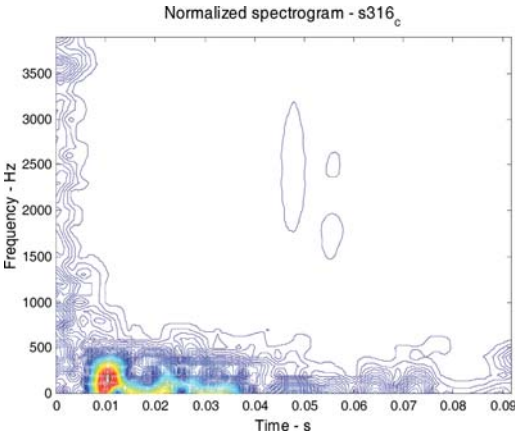

Figure 7. Spectrogram of the vertical component of the CH 13,5 m depth trace.

13,5 m corresponds to a minimum V_S value, following a maximum value attained at depth 10,5 m where initially the water level was thought to be situated. Between depths 10,5 m and 13,5 m there seems to be a gradual increase in the soil water content, to which corresponds a decreasing in both the matrix suction effects and the effective confinement stress accompanied by a drop in the soil stiffness (G_0 local minimum). In this sense both P- and S-waves are affected by the varying dynamic response of the soil influenced by the saturation condition and the related inter-granular capillary forces (Stokoe, K. & Santamarina, C., 2002).

Figure 8 shows the receiver-gather of the 12 vertical component HPB filtered traces for the shot-point at 10,5 m depth. The observed energetic S-waves arriving sequentially to the receivers above and under the shot-point depth would be fitted (first arrival loci) by a hyperbola corresponding to an unexpectedly high velocity, incompatible with the conventional CH profile S-waves arrival times, fitted by the hyperbola tSd.

This occurrence can be explained assuming the borehole cemented casing, above and under the shot-point, acting like an emitter of S_{HV} waves increasingly delayed by a time interval corresponding to the seismic energy vertical travel time through the PVC casing and grout sealing zone. The numerical model of this hypothesis for different depths fits well the observed CH arrival times using for instance a seismic vertical velocity of 5000 m/s.

The CH observed and predicted arrival times are shown in Figure 9, for the 10,5 m receiver-gather and vertical distances, Z, corresponding to depths between 3 m ($Z = -7{,}5$) and 15 m ($Z = 4{,}5$).

The referred effect, practically acts like a virtual continuous shot-line apparently within a significant useful distance around the shot-point, in this particular case about 12 m.

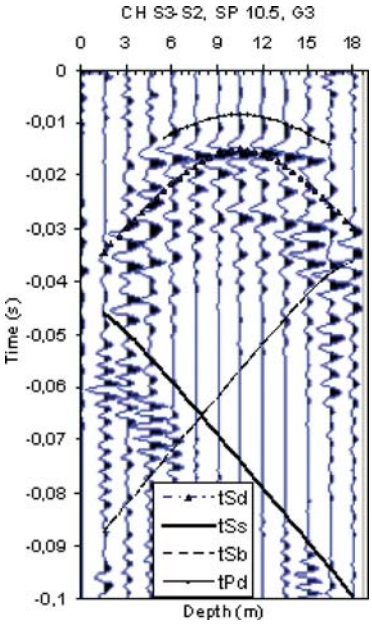

Figure 8. Shot-point 10,5 m vertical component receiver-gather (normalized HPB filtered traces) overlaid by model hyperbolae.

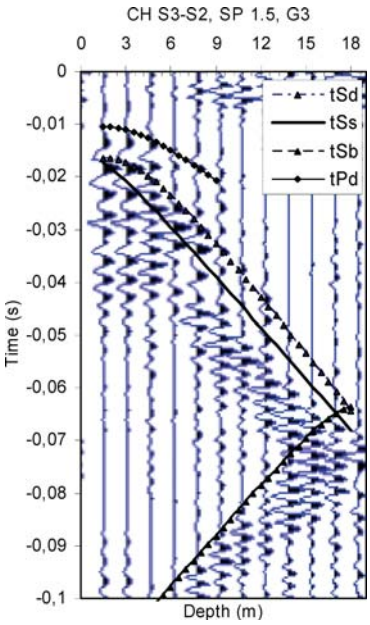

Figure 10. Shot-point 1,5 m vertical component receiver-gather (normalized HPB filtered traces) overlaid by model hyperbolae.

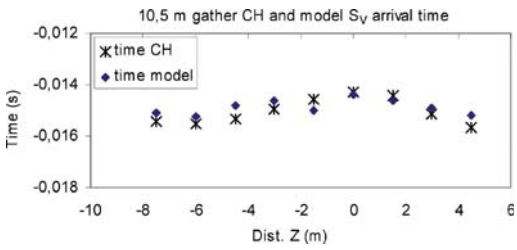

Figure 9. CH observed and predicted arrival time values.

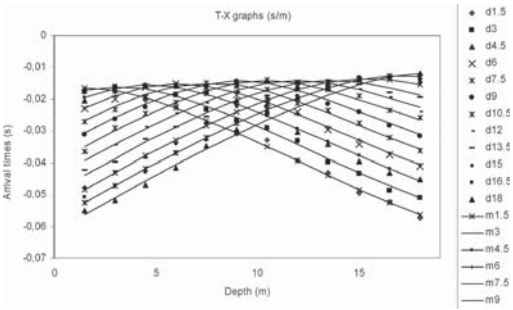

Figure 11. T-X graphs of individually picked traveltimes globally adjusted.

Figure 10 shows the receiver-gather of the 12 vertical component HPB filtered traces for the shot-point at 1,5 m depth, showing very clearly the supposedly reflected events.

The travel time picking was carried out interactively using both an overall model based on interval velocities and each individual trace.

Figure 11 shows an example of T-X graphs of individually picked traveltimes globally adjusted using Excel worksheet and the built-in Solver optimization codes.

The mentioned procedure was used both to validate the picked travel time data as well as to obtaining a global optimized model.

2.3 *Tomographic imaging*

The tomographic velocity imaging was performed using the package Divine, V_S 2.6 available with the Simultaneous Iterative Reconstruction Technique, SIRT, and the Algebric Reconstruction Technique, ART, based on first-arrivals travel times (Pessoa, M., 1994).

The inversion procedure determines a matrix of seismic velocities assumed constant within each cell.

The final 2D continuous velocity distributions are obtained after interpolating the initial velocity matrixes into a denser grid. The S3-S2 tomographic

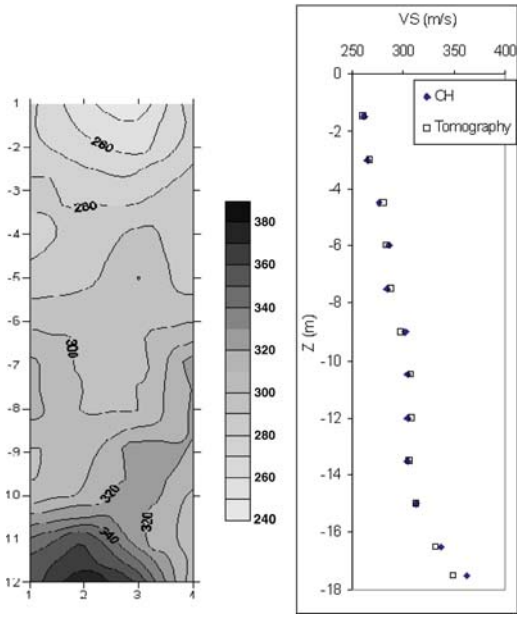

Figure 12. Left: S3-S2 section tomographic image based on a 4 × 12 cells grid. Right: conventional and tomographic V_S profiles ($R^2 = 0{,}988$).

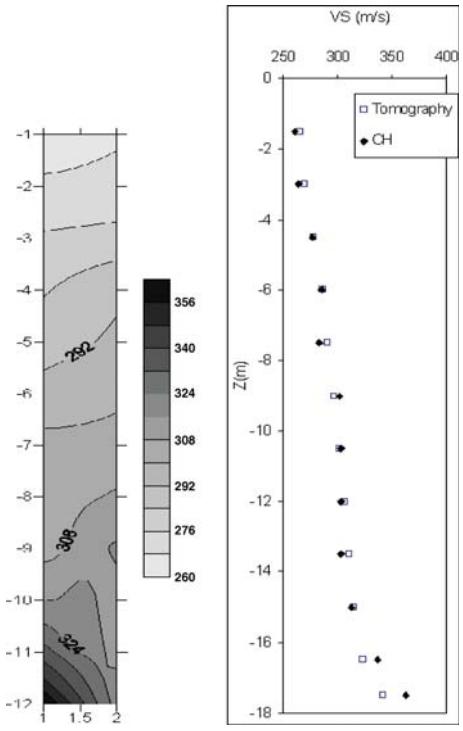

Figure 13. Left: S3-S2 section tomographic image based on a 2 × 12 cells grid. Right: conventional and tomographic V_S profiles ($R^2 = 0{,}978$).

images of Figures 12 and 13 were obtained respectively with initial 4 × 12 and 2 × 12 cells grids.

The compatibility between the tomographic models and the initially obtained 1D conventional CH profile can be assessed by comparing a tomographic average V_S model, with the 1D conventional CH profile (right images on Figures 12 and 13). The following correlation coefficients were obtained: $R^2 = 0{,}988$ and $R^2 = 0{,}978$, respectively.

It is also worth mentioning the fact that the tomographic images are globally very much in accordance with previous obtained results (Almeida et al., 2004; Carvalho et al., 2004; Viana da Fonseca et al., 2004, 2006).

In future work there is the intention of integrating in the velocity inversion processes, reflected and conversion mode events namely at the surface and in the bedrock, as virtual shot-points; this way the overall section ray density will be increased, especially in zones where the cells have lower ray density.

3 CONCLUSIONS

Results based on data from various geophysical, mechanical and laboratory methods/tests applied to the investigation and characterization of ISC'2 FEUP experimental site were presented in precedent studies.

However, seismic CH tomographic data had not yet been processed. The present study reports CH data treatment/processing procedures previous to the velocity inversion leading to the final presented tomographic images. Some aspects and features of the used seismic wavefield, considered relevant for the characterization of the related tomographic section are also discussed and interpreted.

The tomographic images show in average a very good agreement with the previously obtained conventional CH profile as well as with the overall spatial distribution of V_S resulting from other applied seismic methods namely seismic reflection and refraction.

In future work it is intended to verify the advantage of including in the velocity inversion process information from virtual sources namely related to reflections and PVC case/grout effects as well as P-wave velocity inversion taking in consideration interpreted as P-wave related high frequency events, inhere discussed.

REFERENCES

Almeida, F., Hermosilha, H., Carvalho, J.M., Viana da Fonseca, A. and Moura, R., 2004, ISC'2 experimental site investigation and characterization – Part II: From SH

waves high resolution shallow reflection to shallower GPR tests. *Geotechnical and Geophysical Site Characterization. Ed. A. Viana da Fonseca & P.W. Mayne*. Millpress, Rotterdam

Berge, P. and Bonner, B. (2002), Seismic velocities contain information about depth, lithology, fluid content, and microstructure.

Berge, P.A., and Bonner, B.P., 2002, Seismic velocities contain information about depth, lithology, fluid content, and microstructure: UCRL-JC-144792, proceedings of the Symposium on the Application of Geophysics to Engineering and Environmental Problems, Las Vegas, NV, Feb. 10–14, 2002, sponsored by the Environmental and Engineering Geophysical Society, also submitted to the Journal of Environmental and Engineering Geophysics.

Carvalho, J.M., Viana da Fonseca, A., Almeida, F. and Hermosilha, H., 2004, ISC'2 experimental site invest.and characterization – Part I: Conventional and tomographic P and S waves refraction seismics vs. electrical resistivity. Geotechnical & Geophysical Site Characterizaton. Ed. A. Viana da Fonseca & P.W. Mayne. pp. 433–442. Millpress, Rotterdam.

Wang, Y. and Rao, Y., 2006, Crosshole seismic waveform tomography – I. Strategy for real data application. Geophys. J. Int. 166, 1224–1236.

Pessoa, M., 2004. Aplicação de técnicas tomográficas à prospecção sísmica entre furos de sondagem, Relatório 27/94 – NP, LNEC, Departamento de Geotecnia.

Stokoe, K.H. and J.C. Santamarina, 2000, Seismic-Wave-Based Testing in Geotechnical Engineering, GeoEng 2000, Melbourne, Australia, November, pp. 1490–1536. (State-of-the-Art).

Viana da Fonseca, A., Carvalho, J., Ferreira, C., Tuna, C., Costa, E. and Santos, J., 2004, Geotechnical characterization of a residual soil profile: the ISC'2 experimental site, Porto. Geotechnical & Geophysical Site Characterizaton. Ed. A. Viana da Fonseca & P.W. Mayne. pp. 1361–1370. Millpress, Rotterdam.

Viana da Fonseca, A., Carvalho, J., Ferreira, C., Santos, J.A., Almeida, F., Pereira, E., Feliciano, J., Grade, J., Oliveira, A., Characterization of a profile of residual soil from granite combining geological, geophysical and mechanical testing techniques. "Geotechnical and Geological Engineering" (2006) 24: 1307–1348, Springer 2006.